JOURNAL OF COMPUTATIONAL PHYSICS 95, 450–476 (1991)

Adaptive Grid Generation from Harmonic Maps on Riemannian Manifolds

ARKADY S. DVINSKY

Creare Inc.,
Hanover, New Hampshire 03755

Received February 13, 1989; revised April 13, 1990

In this paper we describe a new method for generation of solution adaptive grids based on harmonic maps on Riemannian manifolds. The reliability of the method is assured by an existence and uniqueness theorem for one-to-one maps between multidimensional multiconnected domains. We formulate an adaptive Riemannian metric consistent with this theorem. Several examples demonstrating application of the developed procedure are provided. © 1991 Academic Press, Inc.

1. INTRODUCTION

The grid is an integral part of finite-difference and finite element models. It is known that the efficiency of discrete models is greatly enhanced when they are constructed using natural coordinate systems and when a regular pattern of connectivity between grid nodes is present. These two requirements are satisfied when the grid is obtained by coordinate transformation so that the boundaries of the modeled domain are represented by constant coordinate lines or surfaces. In addition to adapting to the boundaries, the coordinate transformation can be made to adapt to important features of the solution, such as singularities and boundary layers. Such an adaptation is done either prior to solving the numerical problem on the basis of a priori information about the solution or dynamically by adapting to the evolving solution. In this paper we are concerned only with the latter type of adaptation.

Among the methods which generate grid by solving partial differential equations, two main approaches can be distinguished. The first approach was proposed by Godunov and Prokopov in 1972 and is based on reparameterization of Laplace grid generator by Winslow [23] to enable grid control. Further development of refinement of this approach has been made by Joe Thompson and co-workers [22]. Dale Anderson [3] recently proposed a particular form of the source terms in the Poisson equations which tend to equidistribute certain weights on the grid. This approach seems to be particularly promising for adaptive grid generation. Although Godunov and Prokopov formulated their grid equations to ensure existence and uniqueness of one-to-one maps, this is generally not possible for Poisson equations.

0021-9991/91 $3.00
Copyright © 1991 by Academic Press, Inc.
All rights of reproduction in any form reserved.

Another extension of Winslow's method was proposed by Yanenko with co-authors in the mid-seventies [24, 15]. They formulated a minimization problem by linearly combining several functionals that measure desired grid properties. By varying the magnitude of the coefficients in this linear combination, different mapping properties are emphasized. It is important to note, that one of the functionals in this method is the functional which measures deviation from conformality. The corresponding Euler–Lagrange equations for such a functional are Laplacians. In cases where the "conformal" functional is not used, the rest of the functionals in the combination are often not convex and this leads to Euler–Lagrange equations which have non-unique solutions. (Non-uniqueness, of course, does not preclude one from using these non-convex functionals for grid generation.) A particular form of this approach was shown by Brackbill and Saltzman [5], who used the conformality functional in combination with the orthogonality and cell size measure functionals. Roache and Steinberg [18] and Castillo [6] have contributed to further understanding and refinement of this technique.

The variational methods are a natural framework for solution adaptive grids. However, the complexity of the Euler–Lagrange equations resulting from the Yanenko approach significantly exceeds that of the Poisson equation method. In addition, the method requires the use of empirically adjustable coefficients and, in general, does not assure one-to-one maps.

The importance of existence and uniqueness results for one-to-one maps has been realized by researchers in numerical grid generation [16]. Thus the reliability of the Godunov–Thompson grid generating system, which is based on Poisson equations, was argued on the basis of this system being "not too far" from the basic grid generating system, the Laplace equations, for which such proofs have been established [8, p. 504]. The Laplace equations, however, provide no control over the grid and hence cannot be used for adaptive grid generation.

In this paper we present a new adaptive grid method, the reliability of which is established by an appropriate theorem (Section 3). The method can be viewed as yet another generalization and extension of Winslow's method. However, unlike the methods discussed above, which *add* terms or functionals to the basic Winslow grid generator, the present approach uses a single functional to accomplish the adaptive mapping. The critical points of this functional, which is to be defined in Section 3, are harmonic maps. In addition to a concise formulation, the harmonic maps have another important advantage—an existence and uniqueness theorem for one-to-one maps (this is a conjecture in three dimensions). This ensures reliability of the harmonic map-based grid generators.

The following sections provide the motivation for this research (Section 2), introduce the necessary background including sufficient conditions for existence and uniqueness of harmonic maps (Section 3), discuss and illustrate the concepts presented in the previous section on simple examples (Section 4), formulate adaptive Riemannian metrics (Section 5), show examples of adaptive grids for a convection–diffusion equation (Section 6), and summarize the work done (Section 7).

2. Motivation

Before embracing the mathematical complexities necessary for a general treatment of harmonic maps, we first consider an heuristic example to illustrate some of the ideas and motivation behind this work. Consider a boundary value problem

$$\begin{aligned} Lu &= f(x) \qquad \text{in } D \\ lu &= \phi(x) \qquad \text{at } \partial D. \end{aligned} \tag{1}$$

We assume that the solution of (1) is "complicated" when expressed as a function of x and hence we seek a new coordinate, z, $z = z(x)$ such that u is not "complicated" when written in terms of z. We define the function behavior as "complicated" when $\hat{u}_{zz} \gg 1$ and as not "complicated" when $\hat{u}_{zz} \ll 1$, where $u(x(z)) = \hat{u}(z)$. Using the chain-rule we obtain

$$u_{xx} = \hat{u}_z z_{xx} + \hat{u}_{zz} z_x^2. \tag{2}$$

By definition, we require $\hat{u}_{zz} = (u_{xx} - \hat{u}_z z_{xx})/z_x^2 \ll 1$. After some algebra we obtain a sufficient condition for $\hat{u}_{zz} \equiv 0$ which is given by

$$x_{zz} + \frac{u_{xx}}{u_x} x_z^2 = 0. \tag{3}$$

Equation (3) is a one-dimensional harmonic map. The calculation of $z = z(x)$ from (3) assures that the solution of (1) in the new coordinates is simple.

Consider a one-dimensional analog of convection–diffusion equation

$$u_{xx} + Ru_x = 0 \tag{4}$$

with the boundary conditions

$$u(0) = 0, \qquad u(1) = 1. \tag{5}$$

The exact solution of (4)–(5) is

$$u = \frac{e^{-Rx} - 1}{e^{-R} - 1}. \tag{6}$$

When parameter R is large, this problem exhibits a boundary layer of thickness $O(1/R)$ at the $x = 0$ boundary. This is one of the simplest singular perturbation problems, since as $R \to \infty$ the solution approaches a step function.

We wish now to numerically solve for u as a function of x in the domain X, $\forall x \in [0, 1]$. Since we know that the solution is quite "complicated" when written as a function of x, to facilitate the numerical solution we seek a new coordinate

system, z, such that u is not "complicated" when expressed as a function of z. Let us now transform Eq. (4) to the new coordinates, which gives

$$\frac{u_{zz}}{x_z^2}+\frac{1}{x_z}\left(R-\frac{x_{zz}}{x_z^2}\right)u_z=0 \tag{7}$$

with the boundary conditions

$$u(z=1)=0, \qquad u(z=N)=1, \tag{8}$$

where $\forall z \in [1, N]$, N is a natural number greater than 2.

By inspection, the optimal mesh for this equation is obtained from

$$x_{zz}-Rx_z^2=0 \tag{9}$$

and the boundary conditions $x(1)=0$ and $x(N)=1$:

$$x=-\frac{1}{R}\ln\frac{e^{-R}-N-ze^{-R}+z}{1-N}. \tag{10}$$

Note that Eq. (9) could have been obtained directly from Eq. (3) by observing that $u_{xx}/u_x=-R$. The solution u is indeed simple as a function of z:

$$u(z)=\frac{1-z}{1-N}, \tag{11}$$

where $z=1, 2, ..., N$. Let us solve Eq. (7) on z numerically. Applying central differences we obtain

$$y_{i+1}-2y_i+y_{i-1}=0. \tag{12}$$

The solution of (12) with the boundary conditions $u(i=1)=0$ and $u(i=N)=1$ is given by

$$u(i)=\frac{1-i}{1-N}, \tag{13}$$

which is exactly the same as (11). Therefore by numerically solving this singular perturbation problem on a specially designed grid we have been able to obtain an exact solution.

In general, the ratio u_{xx}/u_x depends on x which couples the grid equations together with the equations describing the physics. To simplify the problem one then calculates grid based on the old solution of the physical problem thus effectively decoupling the two. In such a case, as the solution of the grid equation proceeds, the physical solution should be reinterpolated to new grid locations.

3. Harmonic Maps: Definitions and Existence Theorem

In this section we introduce harmonic maps and state sufficient conditions for their existence and uniqueness. A correct presentation of this subject demands considerably more involved mathematics than is required elsewhere in this paper. The readers who are primarily interested in practical applications of this method may wish to refer directly to Section 4, where the main results of this section are reiterated, discussed, and illustrated on simple examples.

The theory of harmonic maps is relatively new. Harmonic maps have been defined and named by Fuller [9]. However, until Eells and Sampson's [7] fundamental work, this area of mathematics had not received much study. Since that paper, harmonic maps have attracted considerable attention both from mathematicians and also physicists (e.g., [17]). The develoment of the theory followed two paths: the study of the existence, uniqueness, and regularity (e.g., [20, 12, 14]) and the applications of harmonic maps to different areas in mathematics (see, for example, the proof of the contractibility of Teichmuller space by Jost [13]). In this work we are primarily concerned with the first path.

Suppose that X and Z are Riemannian manifolds of dimension n with metric tensors $g_{\alpha\beta}$ and G_{ij} in some local coordinates x^n and z^n, respectively. If $x: Z \to X$ is a C^1 map, we define the energy density by

$$e(x) = \frac{1}{2} G^{ij}(z)\, g_{\alpha\beta}(x) \frac{\partial x^\alpha}{\partial z^i} \frac{\partial x^\beta}{\partial z^j}, \tag{14}$$

where the standard summation convention is assumed. The total energy associated with the mapping x is then

$$E(x) = \int_Z e(x)\, dZ. \tag{15}$$

If x is of class C^2, $E(x) < \infty$, and x is a critical point of E, then x is called harmonic. That is, harmonic maps are critical points of the energy functional, where the energy density is defined in terms intrinsic to the geometry of the domain, the target manifold, and the map between them. The corresponding Euler–Lagrange equations are given by

$$\frac{1}{\sqrt{G}} \frac{\partial}{\partial z^k} \sqrt{G}\, G^{kj} \frac{\partial x^\lambda}{\partial z^j} + G^{kj} \Gamma^\lambda_{\alpha\beta} \frac{\partial x^\alpha}{\partial z^k} \frac{\partial x^\beta}{\partial z^j} = 0, \tag{16}$$

where $G = \det(G_{ij})$ and $\Gamma^\lambda_{\alpha\beta}$ are Christoffel symbols of the second kind on x. Thus, we have obtained a system of partial differential equations, where the principal part is a Laplace–Beltrami operator, while the non-linearity is quadratic in the gradient of solution.

Next we formulate sufficient conditions for existence and uniqueness of harmonic maps. The theorem shown below, referred to here as the HSY theorem, is due to Hamilton [11] and Schoen and Yau [19].

HAMILTON–SCHOEN–YAU THEOREM. *Let* (X, ρ), (Z, v) *be two Riemannian manifolds with boundaries* ∂X, ∂Z *and* $\phi: X \to Z$ *be a diffeomorphism. For any map* $f: X \to Z$ *such that* $f|_{\partial X} = \phi|_{\partial X}$ *we define* $E(f) = \int_X \|df\|^2 \, dX$. *We say that* f *is harmonic if it is an extremal of* E.

THEOREM. *If the curvature of* Z *is nonpositive, and* ∂Z *is convex (with respect to metric* v*), then there exists a unique harmonic map* $f: X \to Z$ *such that* f *is an homotopy equivalent to* ϕ. *In other words, one can deform* f *to* ϕ *by constructing a continuous family of maps,* $g_t: X \to Z$, $t \in [0, 1]$, *such that* $g_0(x) = \phi(x)$ *and* $g_1(x) = f(x)$ *and* $g_t(x) = \phi(x)$, $\forall x \in \partial X$, $t \in [0, 1]$.

The HSY theorem is valid for n-dimensional, multiconnected domains. For certain choices of the metrics the theorem reduces to the maximum principle for linear elliptic partial differential equations (e.g., [4]).

4. APPLICATION OF THE HSY THEOREM

The HSY theorem states sufficient conditions for existence and uniqueness of harmonic maps. For further discussion it will be convenient to associate the manifolds mentioned in the theorem with the physical and computational domains normally used in grid generation. Suppose that X is a given physical domain and Z is a constructed (computational or logical) domain; then according to the theorem, an $Z \to X$ map exists when the following two conditions are satisfied:

1. The curvature of X is non-positive, and
2. ∂X is convex.

The first condition can be readily satisfied by defining an appropriate metric, for example Euclidean, on X. (The Euclidean space is "flat"; i.e., it has zero curvature.) If, in addition, the boundary of the physical domain is convex, the $Z \to X$ mapping can be always accomplished. In cases when ∂X is not convex, however, the existence and uniqueness of the map is not assured.

The $Z \to X$ mapping is accomplished by numerically solving Eq. (16). We used second-order central differences for the second derivatives. Using the second-order central differences for approximation of the first derivative, however, causes appearance of oscillating modes for high values of $G^{kj}\Gamma^{\lambda}_{\alpha\beta}$. One way to eliminate these modes is to use one-sided (upwind) first-order accurate differences for the first derivatives. But accuracy of this approximation is often not sufficient, especially for 2D and 3D problems where one is often forced to use rather coarse grids. (We assume that (16) describes a nearly optimal coordinate transformation and hence its accurate solution *is* important.) A simple remedy in this case is to use a product of forward and backward one-sided first-order accurate differences, for example, in one dimension $x_z^2 \approx (x_{i+1} - x_i)(x_i - x_{i-1})$. The resulting approximation of the nonlinear term is then second-order accurate.

We tried several different approaches to linearize (16). The Picard linearization, when the non-linear term is calculated explicitly (e.g., [1]), does not work for large values of $G^{kj}\Gamma^{\lambda}_{\alpha\beta}$. We also tried

$$\frac{1}{\sqrt{G}}\frac{\partial}{\partial z^k}\sqrt{G}\,G^{kj}\frac{\partial x^{\lambda,n+1}}{\partial z^j}+G^{kj}\Gamma^{\lambda}_{\alpha\beta}\frac{\partial x^{\alpha,n+1}}{\partial z^k}\frac{\partial x^{\beta,n}}{\partial z^j}=0,$$

where the superscript n denotes the iteration level, and the Newton linearization

$$\frac{1}{\sqrt{G}}\frac{\partial}{\partial z^k}\sqrt{G}\,G^{kj}\frac{\partial x^{\lambda,n+1}}{\partial z^j}+2G^{kj}\Gamma^{\lambda}_{\alpha\beta}\frac{\partial x^{\alpha,n+1}}{\partial z^k}\frac{\partial x^{\beta,n}}{\partial z^j}-G^{kj}\Gamma^{\lambda}_{\alpha\beta}\frac{\partial x^{\alpha,n}}{\partial z^k}\frac{\partial x^{\beta,n}}{\partial z^j}=0.$$

Both of these procedures worked well in our tests for any value of $G^{kj}\Gamma^{\lambda}_{\alpha\beta}$.

The mapping in the opposite direction, $X\to Z$, as accomplished by solving

$$\frac{1}{\sqrt{g}}\frac{\partial}{\partial x^k}\sqrt{g}\,g^{kj}\frac{\partial z^{\lambda}}{\partial x^j}+g^{kj}\Gamma^{\lambda}_{\alpha\beta}\frac{\partial z^{\alpha}}{\partial x^k}\frac{\partial z^{\beta}}{\partial x^j}=0, \tag{17}$$

where $g=\det(g_{ij})$ and $\Gamma^{\lambda}_{\alpha\beta}$ are Christoffel symbols of the second kind on z. In practice, however, Eq. (17) is inverted to solve for $x^k(z^1, z^2, z^3)$ which makes the resulting equations considerably more complex than the ones used for $Z\to X$ mapping. Equation (17) yields one-to-one maps provided the non-positive curvature and convex boundary are in the computational domain Z. Since Z is obtained by construction, both requirements can usually be satisfied. Therefore in general, it is more advantageous to formulate an $X\to Z$ map, since in such a case a diffeomorphism can always be assured under conditions of the HSY theorem.

The following examples illustrate the above discussion regarding the direction of mapping. Consider Eq. (16) for mapping between Euclidean domains, that is, $g_{ij}=G_{ij}=\delta_{ij}$, where δ_{ij} is the Kronecker delta,

$$x_{\xi\xi}+x_{\eta\eta}=0 \tag{18}$$

$$y_{\xi\xi}+y_{\eta\eta}=0, \tag{19}$$

where $(x, y)\in X$ and $(\xi, \eta)\in Z$. The map shown is $Z\to X$ and, hence, according to the HSY theorem, for the transformation to exist, be unique, and be one-to-one, X must have nonpositive curvature and ∂X must be convex. The first condition is satisfied since we set $g_{ij}=\delta_{ij}$, which implies zero curvature. Then, if ∂X is convex we will be able to obtain a grid independently of the shape of ∂Z. It can be shown, that if Eqs. (18) and (19) are discretized using central differences, the above statement is valid for any grid density, since the *discretized* equations satisfy the maximum principle. Suppose we map domain Z shown in Fig. 1a onto a unit square, domain X. The resulting grid is shown in Figure 2.

If, however, ∂X is not convex, for example like domain Z shown in Fig. 1a, a solution to Eqs. (18), (19) may not exist. In fact, such a mapping was attempted

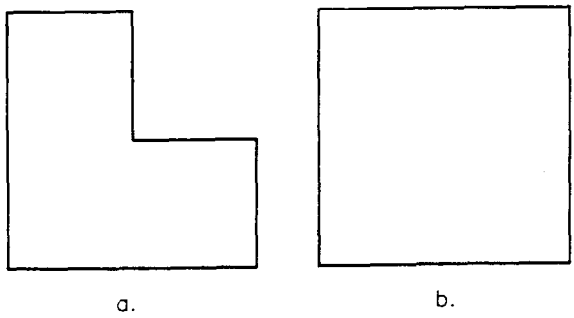

FIG. 1. Examples of domains with a concave boundary (a) and a convex boundary (b).

by Amsden and Hirt [2], who mapped a square logical domain onto a domain similar to the one shown in Fig. 1a. In their calculation the grid folded as it did in our calculation shown in Fig. 3.

Consider now a harmonic map in the opposite direction, $X \to Z$, which is given by a solution to Eq. (17). As in the previous example assume Euclidean metric in both domains. The resulting system is the same as the one originally proposed by Winslow [23],

$$\xi_{xx} + \xi_{yy} = 0 \tag{20}$$

$$\eta_{xx} + \eta_{yy} = 0. \tag{21}$$

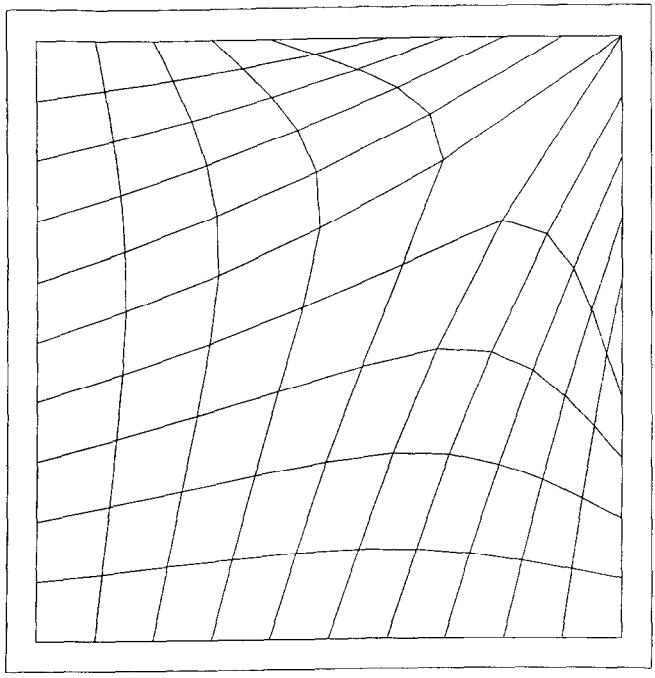

FIG. 2. Mapping of domain shown in Fig. 1a onto domain in Fig. 1b using Eqs. (18) and (19).

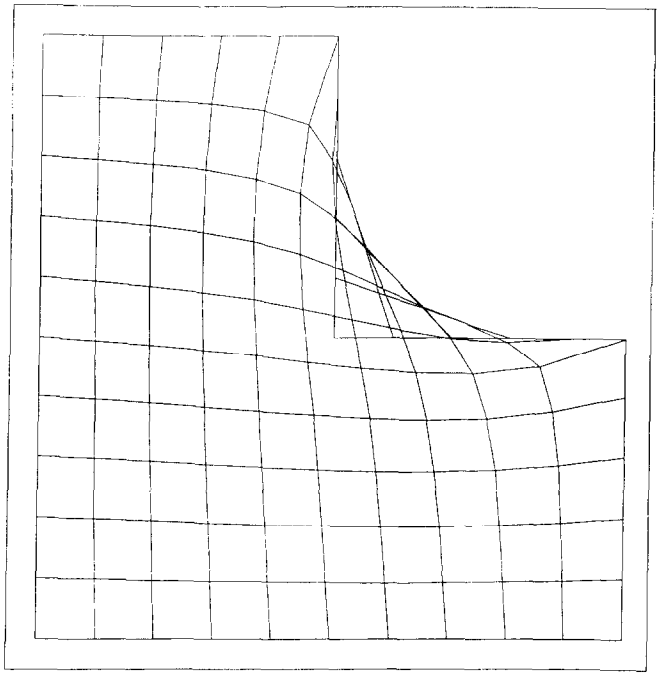

FIG. 3. Mapping of domain shown in Fig. 1b onto domain in Fig. 1a using Eqs. (18) and (19).

A map for Eqs. (20), (21) exists and is a diffeomorphism for convex ∂Z both when (20) and (21) are in differential and in central-difference forms. The usual way to solve (20), (21) is, however, to transform them to logical space variables. The transformation yields the quasilinear system of equations [22]

$$g_{22}x_{\xi\xi} - 2g_{12}x_{\xi\eta} + g_{11}x_{\eta\eta} = 0 \tag{22}$$

$$g_{22}y_{\xi\xi} - 2g_{12}y_{\xi\eta} + g_{11}y_{\eta\eta} = 0, \tag{23}$$

where $g_{22} = x_\eta^2 + y_\eta^2$, $g_{11} = x_\xi^2 + y_\xi^2$, and $g_{12} = x_\xi x_\eta + y_\xi y_\eta$. Although the solution of (22) and (23) should be the same as that of (20) and (21) and, hence, should be a diffeomorphism, it is not obvious that any consistent finite-difference form of (22), (23) produces a diffeomorphism for any grid density. Our experience, however, has shown that (22), (23) are indeed very robust for a wide variety of problems.

Let us consider an interesting example of using (20), (21) and (22), (23) which produces a rather unexpected result. In this example we will attempt to map a square physical domain, Fig. 1b, onto a computational domain in Fig. 1a using (20) and (21). Except for notation, this is the same case we calculated above using $Z \to X$ mapping the result of which, the folded grid, was shown in Fig. 3. Based on this result, we know that Eqs. (20), (21) have no solution either.

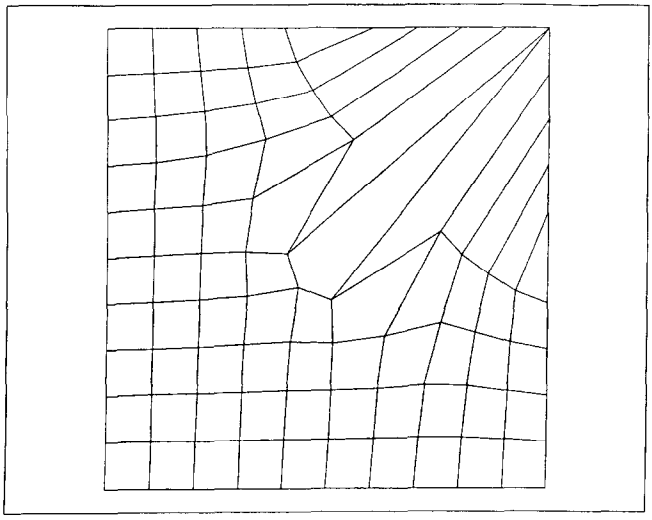

FIG. 4. Mapping of domain shown in Fig. 1b onto domain in Fig. 1a using (20) and (21).

There is a difference, however, between these two cases. As we mentioned above, the usual practice of calculating $X \to Z$ map is to solve the inverse of (20), (21), Eqs. (22), (23). Solving (22), (23) we obtain the map shown in Fig. 4. To our surprise the grid did not fold. The solution to this puzzle turned out to be fairly simple: by inverting (20), (21) the problem has been changed from mapping $X \to Z$ to $Z \to X$. This second problem neatly cuts off the domain where the one-to-two map occurs. Therefore the right-upper corner of the X domain which previously mapped onto outside of Z now has no image inside Z and, hence, is not covered by the grid.

Finally we will revisit the example from Section 2 and consider it in light of the information we learned about harmonic maps. Equation (9) is a one-dimensional version of (16) with $G_{11} = 1$ and $\Gamma^1_{11} = -R$. This mapping is guaranteed by the HSY theorem, since in one dimension ∂X is convex and X, with metrics $g_{11} = ce^{-2Rx}$ where c is some constant, has a nonpositive curvature. Since $u_x \propto e^{-Rx}$ by Eq. (6), the metric can be written in a more meaningful form, namely $g_{11} = c_o u_x^2$. This result will be of use in the next section where we construct an adaptive Riemannian metric.

5. FORMULATION OF RIEMANNIAN METRICS

To utilize the harmonic maps apparatus for adaptive grid generation one has to define Riemannian metrics for the mapped domains. Such a formulation is the subject of this section. For convenience of the discussion, we will differentiate between two types of adaptation: geometrical and physical. We term geometrical adaptation as the process in which the grid clusters in specified (fixed) geometric

locations. The physical adaptation is defined as the usual solution adaptive process in which the grid is adaptively modified in response to evolving physical solution.

To fix the ideas, we first consider a simple problem, where we will attempt to generate a grid clustered around a straight vertical line midway in a square physical domain, X. We will use an $X \to Z$ mapping. The logical domain, Z, for this problem is a rectangle the size of which is determined by the number of grid nodes selected in respective directions. First we want to make sure that the logical domain curvature is non-positive. This is readily accomplished by defining, $G_{ij} = \delta_{ij}$.

The HSY theorem places no restrictions on the physical space metric, g_{ij}, which then can be used for adaptation. Specifically, we want to construct g_{ij} in such a way that it "zooms in" in specified locations to provide a higher solution, while it goes back to its "unperturbed" state away from the special regions. In addition, we want the metric to adapt to the shape of the specified contours, which in this example are just straight vertical lines. For the considered example, such a metric is given by

$$g_{11} = 1 + f(x - x_0) \tag{24}$$

$$g_{22} = 1, \qquad g_{12} = 0, \tag{25}$$

where $x = x_0$ is the selected line of attraction and $f(x - x_0)$ is defined to have a maximum when $x = x_0$ and $f(x - x_0) \to 0$ as $(x - x_0) \to \infty$. An example of such a function for (24) and (25) is given by

$$f(x - x_0) = Ae^{-B(x - x_0)^2}, \tag{26}$$

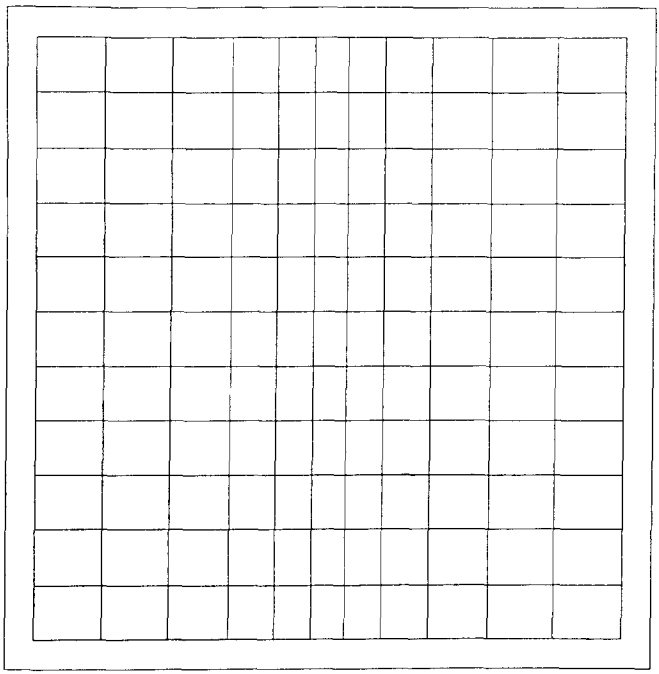

FIG. 5. Grid attraction to $x = 0.5$ using the metrics defined by (24), (25), and (26).

where A and B are positive constants controlling the amplitude and the rate of decay of $f(\cdot)$. Figure 5 shows a grid obtained using (24), (25), and (26). To preserve the one-dimensional character of the problem we used Neumann conditions for Eq. (17) on the horizontal boundaries.

A two-dimensional example is provided by attraction to a circle in the physical domain. Consider a rectangular physical domain and a circle of radius R with its center at (x_c, y_c), so that the entire circle is inside the domain. We want to construct a Riemannian metric which would expand at the rim of the circle and decay to standard Euclidean as the distance from the rim increases. Noting that a circle is a straight line in polar coordinates, we can immediately write the expression for the metric using the results of the previous example,

$$g_{11} = \frac{f(\rho - R)(x - x_c)^2 + (y - y_c)^2}{\rho^2} \tag{27}$$

$$g_{22} = \frac{(x - x_c)^2 + f(\rho - R)(y - y_c)^2}{\rho^2} \tag{28}$$

$$g_{12} = \frac{(x - x_c)(y - y_c)(f(\rho - R) - 1)}{\rho^2}, \tag{29}$$

where $\rho^2 = (x - x_c)^2 + (y - y_c)^2$ and R is the radius of circle. An example of a grid calculated using (29) is shown in Fig. 6.

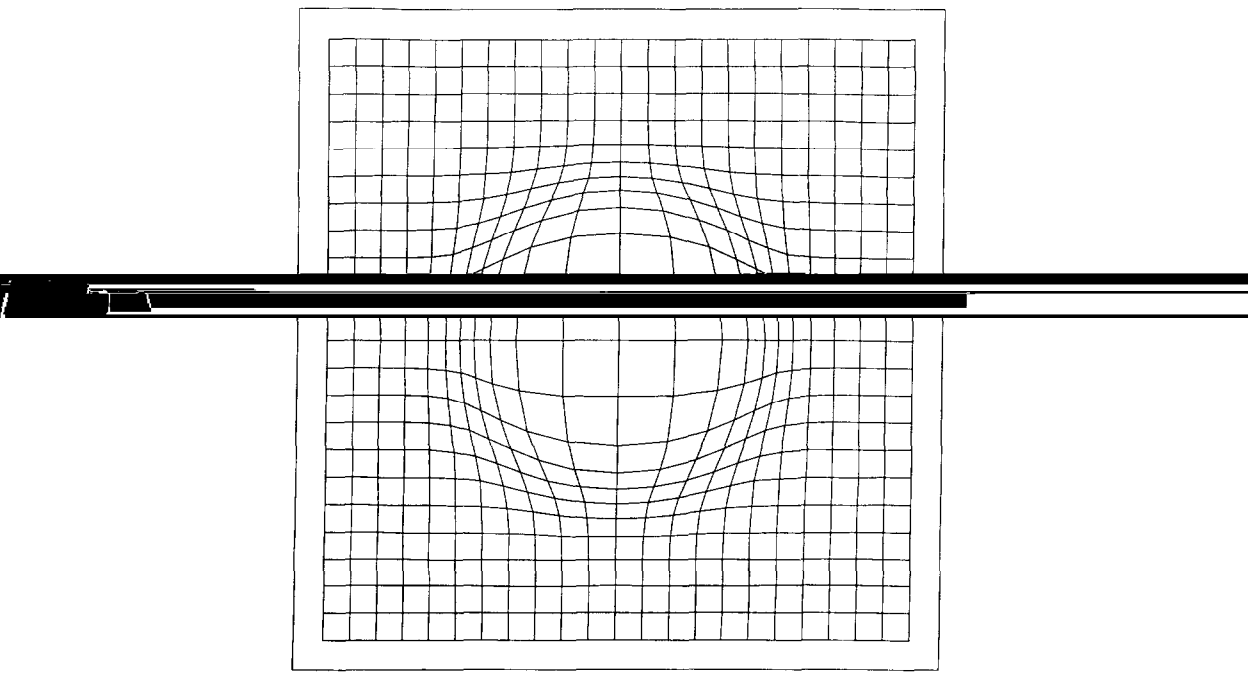

FIG. 6. Grid attracted to $(x - x_c)^2 + (y - y_c)^2 = 0.25^2$ using the metrics from Eq. (29).

These results can be generalized to an arbitrary curve, point, or any combination thereof. Suppose that the attraction locations are given by a function $F(x)=0$, $\{x\}=\{x^1, x^2, x^3\}$. For example, if attraction is required to the n separate curves $F_i(x)=0$, where $i=1, 2, ..., n$, then $F(x)=F_1F_2\cdots F_n$. It then follows that

$$g_{ij}=\delta_{ij}+f(F)\frac{F_{x^i}F_{x^j}}{(\nabla F)^2}, \tag{30}$$

where $f(F)$ is a function of the distance from a given point to $F(x)=0$ such that $f(F)$ increases as the distance tends to zero, and goes to zero as the distance increases, and the subscript denotes a partial derivative with respect to x^i. Thus, the adaptive Riemannian metric consists of an Euclidean, δ_{ij}, and a non-Euclidean part, $f(F)\,F_{x^i}F_{x^j}/(\nabla F)^2$. The non-Euclidean part is in turn a product of the magnification factor, $f(F)$, which controls the magnitude of the metrics and the directional factor, $F_{x^i}F_{x^j}/(\nabla F)^2$, which modifies the magnitude depending on the direction of selected contour lines.

Equation (30) requires a rather expensive calculation of the shortest distance from each grid node, x_0, to $F(x)=0$. This calculation can, however, be readily eliminated if we notice that $F(x_0)$ is a measure of distance from x_0 to $F(x)$. Incidentally, in both previous examples $F(x_0)$ is exactly the shortest distance between x_0 and $F(x)$. Figure 7 shows an example of the grid attracted to a parabola, $y=3(x-0.5)^2$, and hence $F=y-3(x-0.5)^2$, while Fig. 8 depicts grid refined around

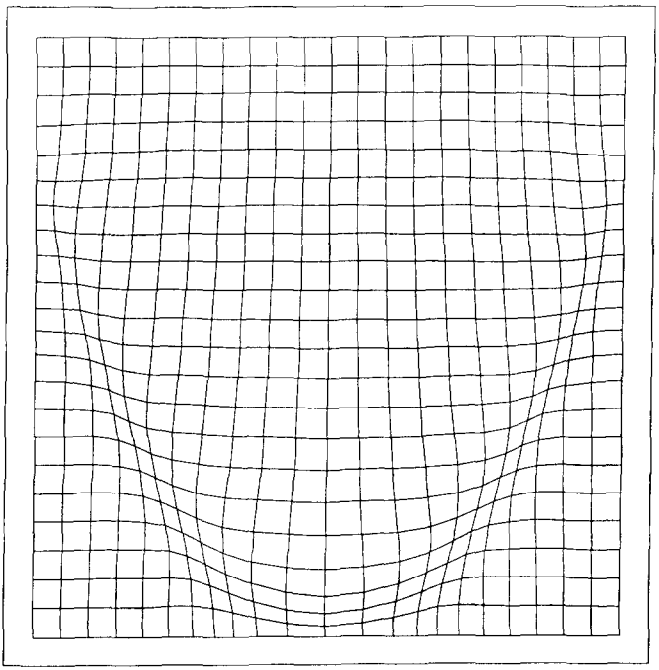

FIG. 7. Grid attracted to a parabola, $y=3(x-0.5)^2$ using the metrics from Eq. (30).

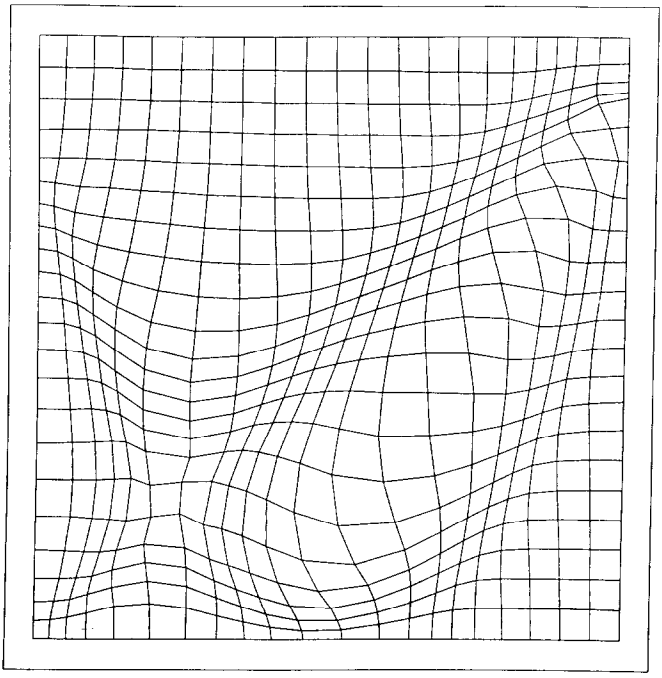

FIG. 8. Grid attracted to a parabola, $y = 3(x-0.5)^2$, and a straight line, $y = x$, using the metrics from Eq. (30).

the parabola and a straight line, $F = (y - 3(x-0.5)^2)(y-x)$. The grids shown in these figures were calculated from Eq. (17) with g_{ij} from (30) and $G_{ij} = \delta_{ij}$.

The procedure for the geometric adaptation described above can be readily extended to the physical adaptation. Suppose one can formulate a scalar function which characterizes and monitors the essential features of the physical problem. Fortunately, this often can be accomplished, since the evolving solution is usually controlled by just a few critical variables. These variables, or some suitable function of them, can then be combined into a single scalar function—the characteristic function. Recall that the expression for Riemannian metrics (30) adapts the metrics to contours of continuously or discretely specified scalar function $F(x)$. Therefore, once the characteristic function is defined, the physical metrics are given by the same expression as the geometric ones. Examples of the physical adaptation are shown in the next section.

6. NUMERICAL EXAMPLES

In this section we apply the concepts presented above to numerical solution of the convection–diffusion equation

$$Ru_x = u_{xx} + u_{yy} + \alpha^2(1 - e^{R(x-1)}) \sin \alpha y \tag{31}$$

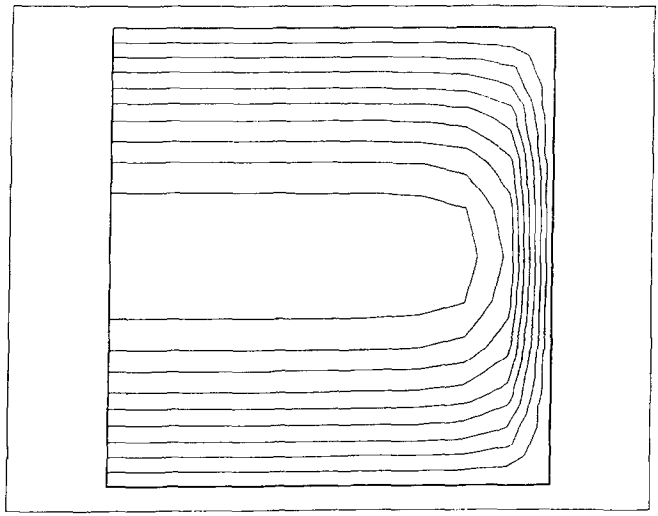

FIG. 9. Contours of u calculated from Eq. (31).

with the exact solution given by

$$u = (1 - e^{R(x-1)}) \sin \alpha y, \tag{32}$$

where R and α are parameters. The solution of (31) is first calculated on a unit square with a uniform mesh. Once the solution is obtained we use it to define a characteristic function which is, in turn, employed to form a Riemannian metric

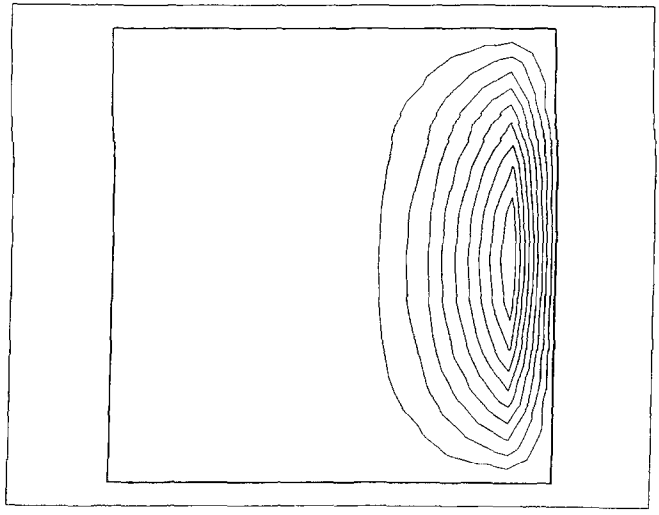

FIG. 10. Contours of E for solution calculated on the uniform grid. $E = 0$ at the boundary and E_{max} is at $(x, y) = (0.9, 0.5)$.

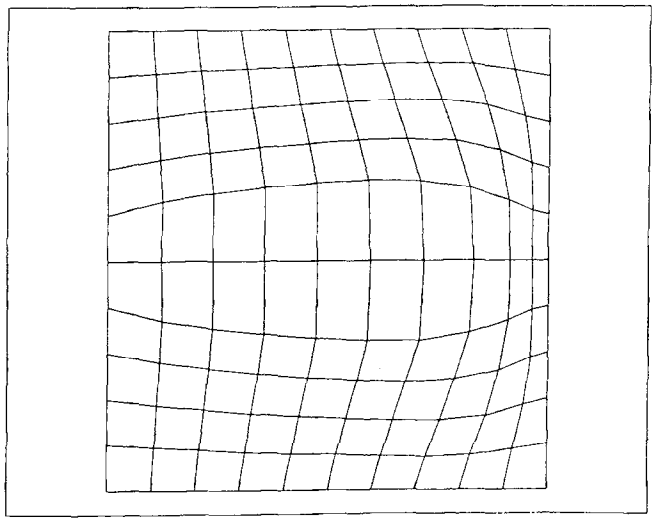

FIG. 11. The adapted grid after the first iteration.

in the physical space. Next, the adaptive grid is obtained from harmonic maps. Equation (31) is then solved on the adapted grid and its solution is compared with the solution obtained on the uniform grid.

Equation (31) is solved as follows. First it is transformed to curvilinear coordinates. Then it is discretized using central differences for second-order derivatives and first-order upwind differences for first-order derivatives. The resulting difference

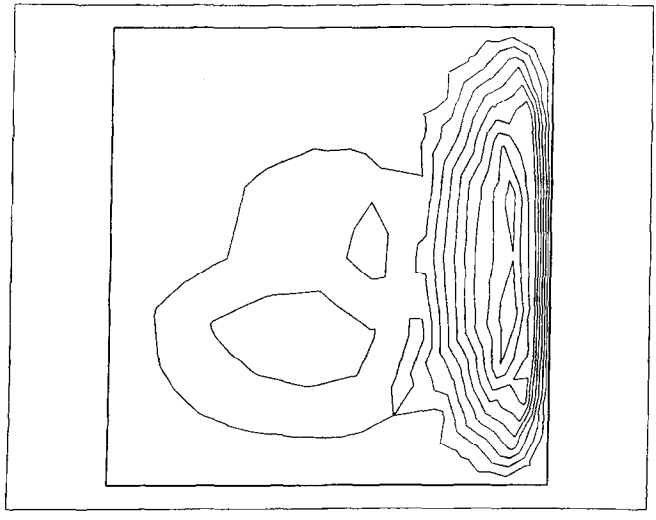

FIG. 12. Contours of E calculated on the grid shown in Fig. 11, E_{max} is at $(x, y) = (0.91, 0.37)$.

equations are solved using red–black successive overrelaxation (SOR) method with Chebyshev acceleration to machine accuracy (6–7 digits on our 32-bit machine).

We use Eq. (17) to calculate the $X \to Z$ map. To assure the non-positive curvature on Z, the metric in the computation domain is assumed Euclidean. As a result the non-linear terms in (17) vanish identically to yield

$$\frac{1}{\sqrt{g}} \frac{\partial}{\partial x^k} \sqrt{g}\, g^{kj} \frac{\partial z^i}{\partial x^j} = 0. \tag{33}$$

Equation (33) is inverted to computational coordinates and discretized using central differences both for the first- and second-order derivatives.

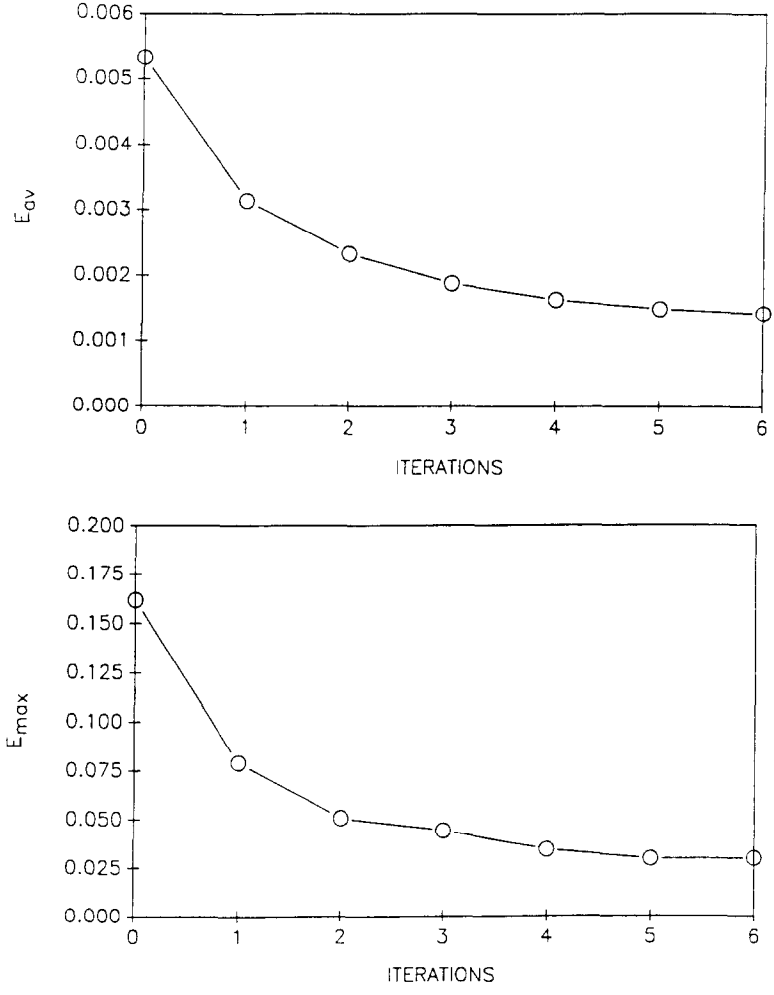

FIG. 13. Convergence history for the first example, E_{av}-panel (a), E_{max}-panel (b).

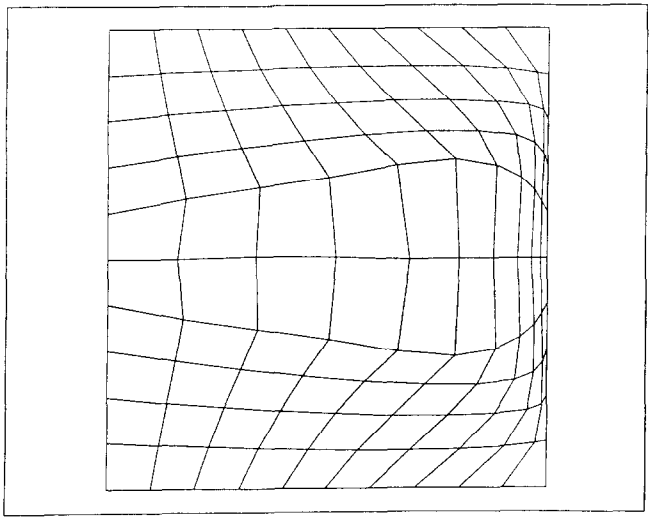

FIG. 14. The adapted grid after the seventh iteration.

In the solution adaptive process the grid and the physics equations are coupled. This often presents a computationally formidable problem which is in practice avoided by decoupling these two processes in one way or the other. In the examples presented below, we will, however, solve Eqs. (33) and (31) in a coupled manner. The coupling will be effected in a "quasi-coupled" fashion where the grid is calculated to convergence for each F field, until the next iteration is started; that is,

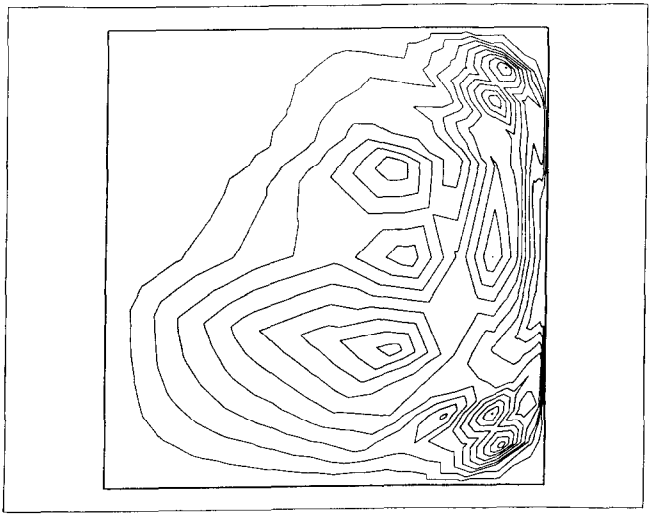

FIG. 15. Contours of E calculated on the grid shown in Fig. 14, $E_{\max}$ is at $(x, y) = (0.88, 0.85)$.

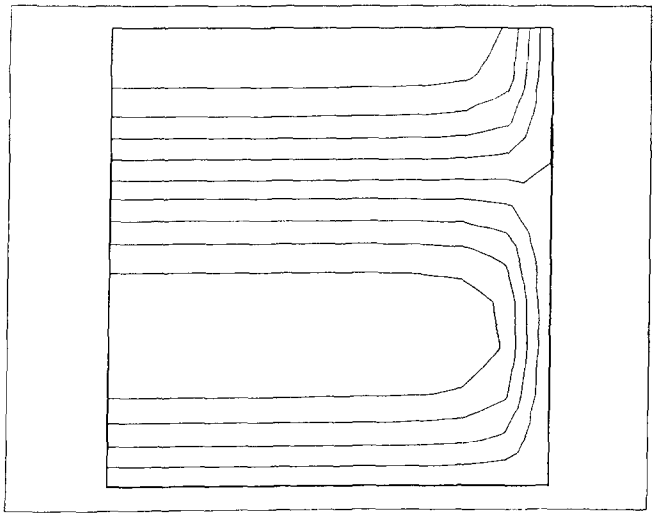

FIG. 16. Contours of u calculated from Eq. (31) for $R = 15$ and $\alpha = 1.5\pi$.

1. solve Eq. (31) to convergence on the latest grid,
2. form the characteristic function from the solution,
3. solve Eq. (33) to convergence using F defined in Step 2,
4. repeat starting with Step 1.

This rather inefficient procedure allows one to see the effects of coupling on the adaptive process. The first iteration of this algorithm corresponds to the often-used

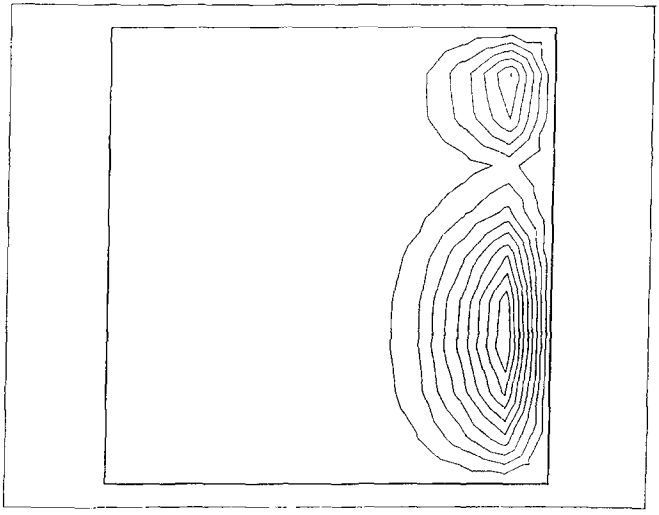

FIG. 17. Contours of E for solution calculated on the uniform grid. $E = 0$ at the boundary and E_{max} is at $(x, y) = (0.9, 0.5)$.

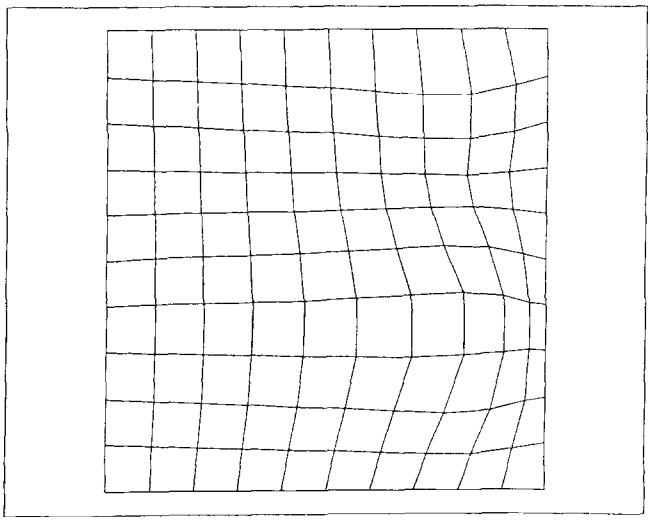

FIG. 18. The adapted grid after the first iteration.

approximate decoupled procedure, where the grid is calculated on the basis of the "old" solution without either recalculation or reinterpolation of that solution to the evolving grid node locations.

To save computer time, we used rather coarse convergence criteria, $(E^{k+1}_{\max} - E^{k}_{\max})/E^{k}_{\max} < 0.05$ and $(E^{k+1}_{\text{av}} - E^{k}_{\text{av}})/E^{k}_{\text{av}} < 0.05$, where $E \equiv (|[u]_{ij} - u_{ij}|)/(1 - e^{-\kappa})$, $[u]_{ij}$ and u_{ij} are the analytical and numerical solutions at the grid node (i, j), respectively; the subscripts denote the maximum error and the average error

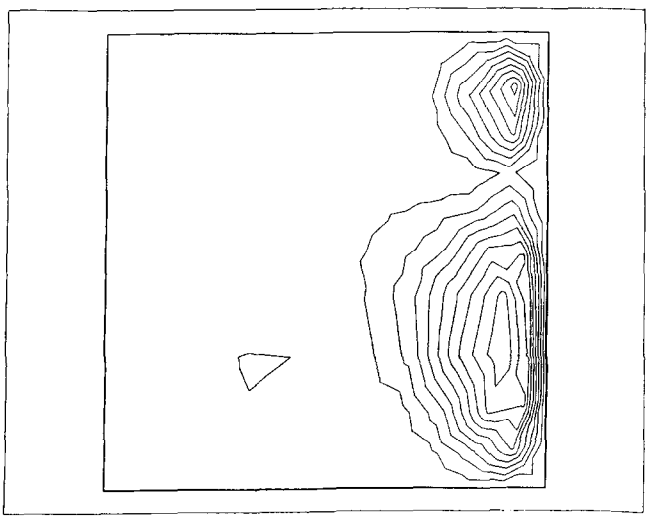

FIG. 19. Contours of E calculated on the grid shown in Fig. 18, $E_{\max}$ is at $(x, y) = (0.90, 0.30)$.

per grid node. In the examples that follow, we used Dirichlet boundary conditions, for example, at the left boundary, Fig. 9, $x_j^1 = 0$, and $x_j^2 = (j-1)/(N-1)$, where $j = 1, 2, ..., N$, N is the number of grid nodes.

In the first example we solve (31) with $R = 15$ and $\alpha = \pi$. The numerical solution calculated on the uniform cartesian 11×11 grid is shown in Fig. 9 and the error is shown in Fig. 10. The maximum and average errors for the solution calculated on the initial grid (the zeroth iteration) are $E_{\max} = 0.162$ and $E_{\text{av}} = 0.00533$, respectively.

In this example, the characteristic function is defined to be the numerical solution itself, that is, $F_{ij} \equiv u_{ij}$, while the attraction function is defined as $f(F) = 1 + \nabla F / \nabla F_{\text{av}}$. The adaptive grid after the first iteration is shown in Fig. 11. The maximum and

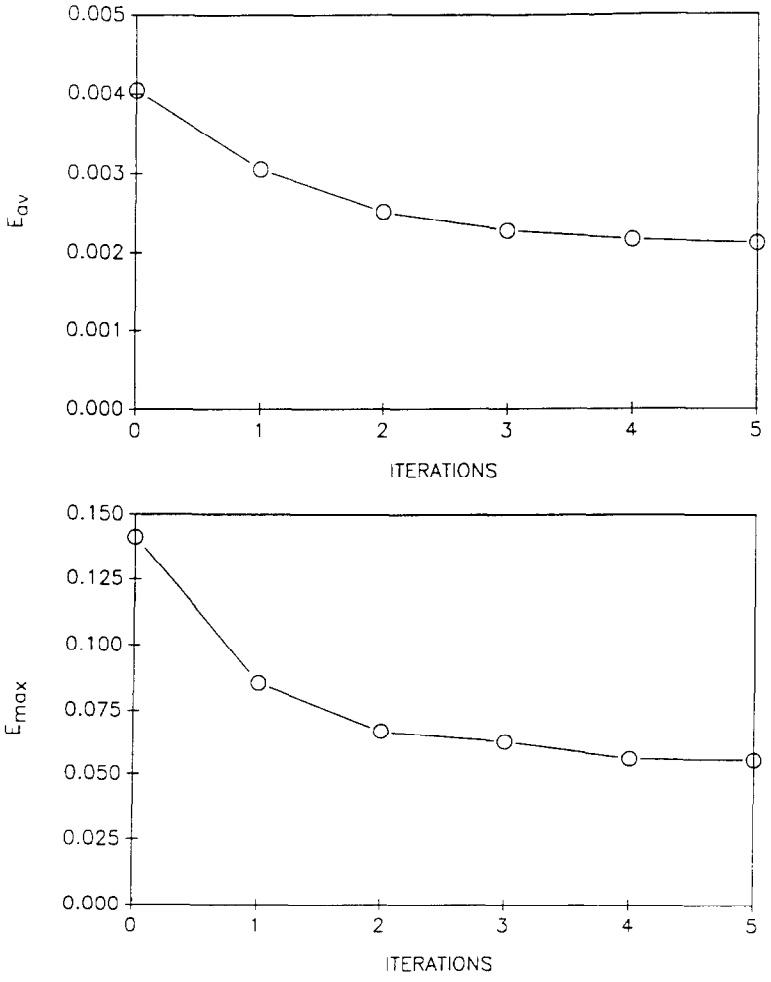

FIG. 20. Convergence history for the second example: E_{av}-panel (a); $E_{\max}$-panel (b).

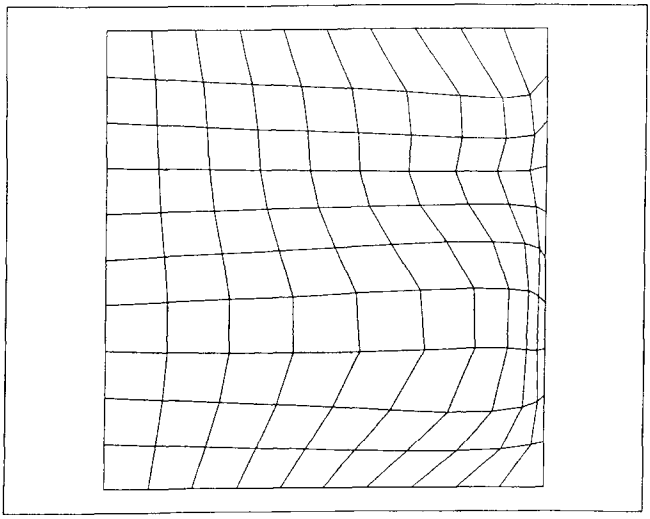

FIG. 21. The adapted grid after the sixth iteration.

average errors for the solution calculated on this grid are $E_{\max} = 0.0791$ and $E_{\text{av}} = 0.00314$, respectively, while the error contours are displayed in Fig. 12. Although we used 11 contours in all figures, sometimes less than 11 contours are visible, which indicates that either maximum and/or minimum coincide with the boundary or the maximum and/or minimum contour is just a single point.

The maximum and average errors for the subsequent iterations are shown in

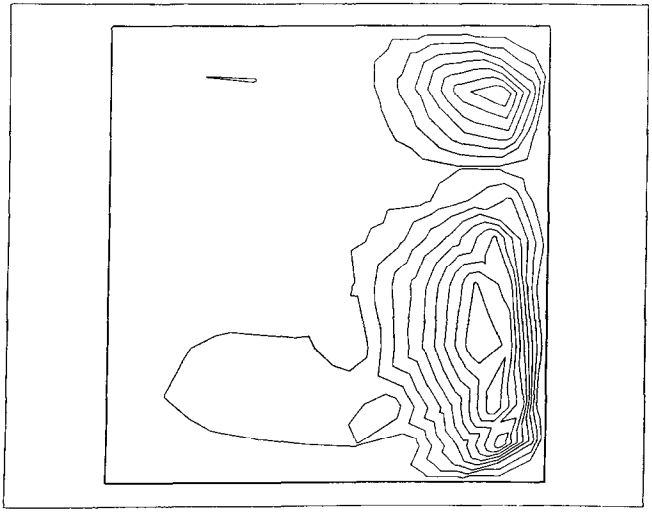

FIG. 22. Contours of E calculated on the grid shown in Fig. 21, $E_{\max}$ is at $(x, y) = (0.84, 0.30)$.

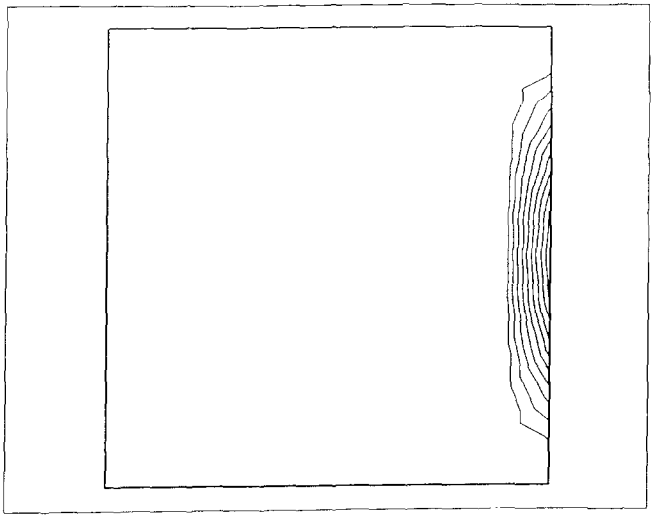

FIG. 23. Contours of $\nabla u \cdot \nabla u$ on the uniform grid, 26 contours are displayed.

Fig. 13. The convergence criteria we stated above were satisfied in the sixths iteration. The corresponding grid is shown in Fig. 14 and the error in Fig. 15.

For the next example, we will change α to $\alpha = 1.5\pi$. The corresponding solution is shown in Fig. 16 and the solution error on the uniform grid in Fig. 17. The adaptive grid after the first iteration is shown in Fig. 18. The maximum and average errors for the solution calculated on the initial grid are $E_{\max} = 0.141$

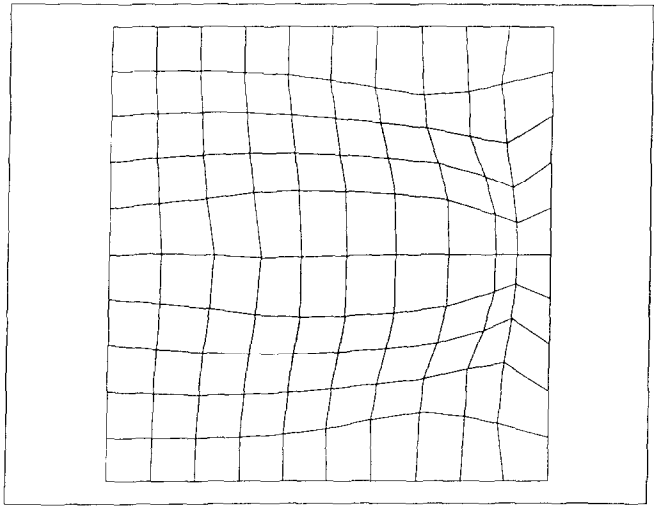

FIG. 24. The adapted grid after the first iteration.

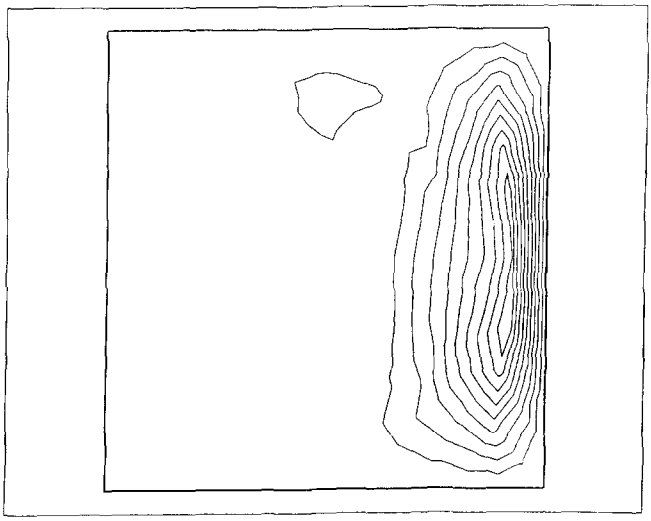

FIG. 25. Contours of E calculated on the grid shown in Fig. 24, E_{max} is at $(x, y) = (0.91, 0.36)$.

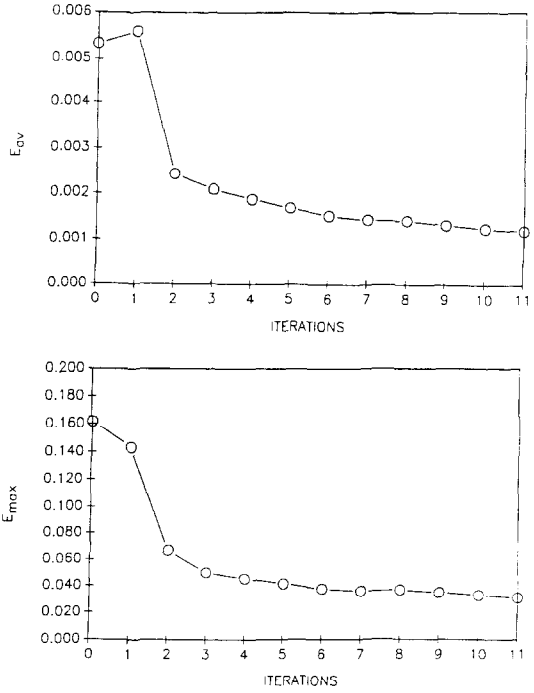

FIG. 26. Convergence history for the third example: E_{av}-panel (a); E_{max}-panel (b).

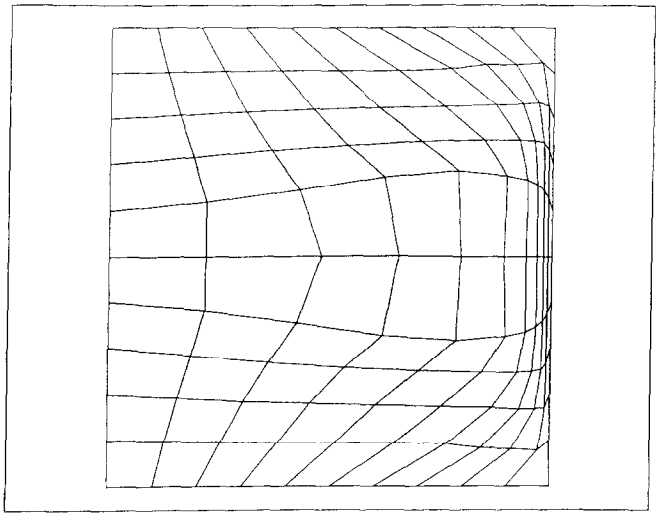

FIG. 27. The adapted grid after the twelfth iteration.

and $E_{av} = 0.00404$, while after the first iteration $E_{max} = 0.0857$ and $E_{av} = 0.00306$, respectively. The error contours for the first iteration are displayed in Fig. 19.

The solution was considered converged after five iterations. The convergence history is shown in Fig. 20. The final grid and the solution error distribution are shown in Figs. 21 and 22, respectively.

In the last example we make several changes. First of all we change the characteristic function to $F = \nabla u \cdot \nabla u$. We also modify the attraction function $f(\cdot)$ to

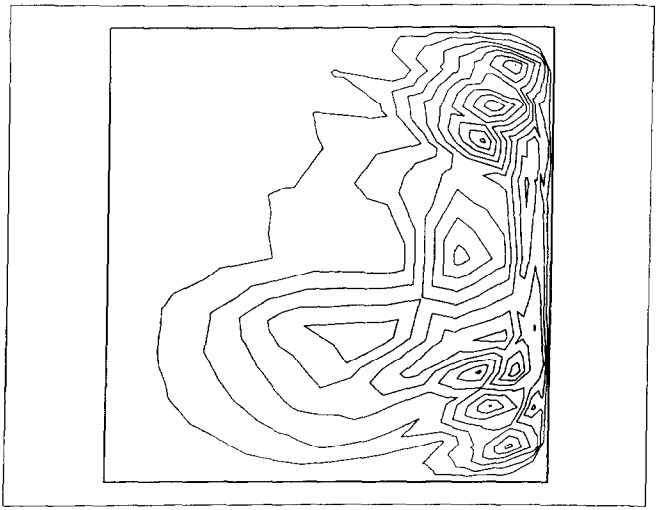

FIG. 28. Contours of E calculated on the grid shown in Fig. 27, E_{max} is at $(x, y) = (0.87, 0.83)$.

$f(F) = 1 + F/F_{av} + \nabla F/\nabla F_{av}$. With these changes we solve again the problem defined in the first example. The contours of F are shown in Fig. 23. The grid after the first iteration and the corresponding error contours are shown in Figs. 24 and 25. In this example the convergence criteria were satisfied in the eighth iteration. However, since in this iteration E_{max} increased, we computed a few more iterations to evaluate the trend. The convergence criteria were met again in the eleventh iteration. The convergence history is shown in Fig. 26. The grid and the error after the eleventh iteration are depicted in Figs. 27 and 28.

The examples shown in this section illustrate how the concepts presented in this paper can be applied to generating adaptive grids for a model diffusion–convection equation. Using simple common-sense definitions for the characteristic and attraction function, we obtained grids which helped to reduce the error in the maximum norm by a factor of five. No adjustable parameters or coefficients have been used in these definitions.

7. Conclusions

In this paper we described a new framework for adaptive grid generation based on the principles of differential geometry. In particular we have utilized the apparatus of harmonic maps for our construction. The described method favorably compares with previously proposed methods in terms of compactness of the governing equations and reliability. The feasibility of the proposed approach was established by formulating adaptive Riemannian metrics in mapped domains and actually performing the numerical mapping. In addition, we investigated the question of existence and uniqueness of one-to-one harmonic maps and formulated sufficient conditions for our application using results by Hamilton [11] and Schoen and Yau [19].

Acknowledgments

The author thanks Professor David Kazhdan of Harvard University for many useful discussions and suggestions during this work. This research has been sponsored by the National Science Foundation Grant ISI 8660378.

References

1. W. F. Ames, *Numerical Methods for Partial Differential Equations*, 2nd ed. (Academic Press, New York, 1977), p. 83.
2. A. A. Amsden and C. W. Hirt, *J. Comput. Phys.* **11**, 348 (1973).
3. D. A. Anderson, in *Proceedings, AIAA 25th Aerospace Siences Meeting, Reno, Nevada*, AIAA-87-0202, 1987.
4. G. Birkhoff and R. E. Lynch, *Numerical Solution of Elliptic Problems* (SIAM, Philadelphia, 1984).
5. J. U. Brackbill and J. S. Saltzman, *J. Comput. Phys.* **46**, No. 3 (1982).

6. J. CASTILLO, thesis, Department of Mathematics and Statistics, University of New Mexico, May 1987.
7. J. EELLS AND J. H. SAMPSON, *Amer. J. Math.* **86**, No. 1, 109 (1964).
8. P. R. EISEMAN, *Annu. Rev. Fluid Mech.* **17**, 487 (1985).
9. F. B. FULLER, *Proc. Natl. Acad. Sci.* **40**, 987 (1954).
10. GODUNOV AND PROKOPOV, *Comput. Math. Math. Phys.* **12**, 182 (1972).
11. R. HAMILTON, *Lecture Notes in Mathematics*, Vol. 471 (Springer-Verlag, New York/Berlin, 1975).
12. S. HILDEBRANDT, *Lecture Notes in Mathematics*, Vol. 1161 (Springer-Verlag, New York/Berlin, 1985).
13. J. JOST, *Lecture Notes in Mathematics*, Vol. 1062 (Springer-Verlag, New York/Berlin, 1984).
14. J. JOST, *Lecture Notes in Mathematics*, Vol. 1161 (Springer-Verlag, New York/Berlin, 1985).
15. V. D. LISEIKIN AND N. N. YANENKO, *Numer. Methods Contin. Mech.* **8**, No. 7, 100 (1977). [Russian]
16. C. W. MASTIN AND J. F. THOMPSON, *Math. Anal. Appl.* **62**, 52 (1978).
17. C. W. MISNER, *Phys. Rev. D* **18**, No. 12, 4510 (1978).
18. ROACHE AND STEINBERG, in *Proc. AIAA 7th CFD Conference, Cincinnati, 1985*, p. 360.
19. R. SCHOEN AND S.-T. YAU, *Invent. Math.* **44**, 265 (1978).
20. R. SCHOEN AND K. UHLENBECK, *J. Differential Geom.* **18**, 253 (1983).
21. J. F. THOMPSON, F. C. THAMES, AND C. W. MASTIN, *J. Comput. Phys.* **15**, 299 (1974).
22. J. F. THOMPSON, Z. U. A. WARSI, AND C. W. MASTIN, *Numerical Grid Generation* (North-Holland, New York, 1985).
23. A. WINSLOW, *J. Comput. Phys.* **2**, 149 (1967).
24. N. N. YANENKO, N. T. DANAEV, AND V. D. LISEIKIN, *Numer. Methods. Contin. Mech.* **7**, No. 4, 157 (1977). [Russian]